Open cell polyurethane foam compression failure characterization and its relationship to morphometry

Ricardo Belda[a,*], Marta Palomar[a], Miguel Marco[b], Ana Vercher-Martínez[a], Eugenio Giner[a]

[a]*Centre of Research in Mechanical Engineering - CIIM, Dept. of Mechanical Engineering and Materials, Universitat Politècnica de València, Camino de Vera, 46022 Valencia, Spain*

[b]*Department of Mechanical Engineering, Universidad Carlos III de Madrid, Avda. de la Universidad 30, 28911, Leganés, Madrid, Spain*

Abstract

Open cell polyurethane foams are often used as cancellous bone surrogates because of their similarities in morphology and mechanical response. In this work, open cell polyurethane foams of three different densities are characterized from morphometric and mechanical perspectives. The morphometric characterization is based on micro computed tomography images analysis, while the mechanical characterization consists of compression tests and finite element models that reproduce them. Moreover, digital image correlation is applied to estimate strain fields at failure to validate the numerical model proposed. We found significant relationships between morphometry and the elastic and failure response. The detailed information about morphometry, elastic constants and strength limits provided in this work can be of interest to researchers and practitioners that often use these polyurethane foams in orthopedic implants and cement augmentation evaluations.

Keywords: Compression fracture characterization, open cell foam, micro-FE, digital image correlation, morphometric characterization

*Corresponding author. Tel.: +34-618243486.
Email address: ribelgon@upv.es (Ricardo Belda)

1. Introduction

Rigid polyurethane foams have been used as cancellous bone surrogate to evaluate orthopedic devices, cement augmentation investigation or mechanical characterization [1–3]. As they do not suffer from biological degradation or dehydration, and due to its lower costs compared to real bone specimens [4], they have become a reliable alternative for cancellous bone-like structure investigations.

One of the first published studies about polyurethane foam characterization was developed by Menges and Knipschild in 1975 [5], where the authors performed a mechanical characterization of closed-cell rigid polyurethane (PUR) foams based on the conception of a simplified beam structure. Gibson et al. went a step further in the study of the mechanics of cellular materials, first in the two-dimensional case [6] and later extended to 3D [7]. The investigation was carried out considering simplified cellular models and defining each of the deformation modes involved: bending, elastic buckling and plastic collapse of the struts. A set of analytical expressions for the mechanical behavior of foams were developed in terms of their geometrical features (strut length and thickness) and then correlated to a relative density parameter [7].

Because of the increasing relevance of polyurethane foams in the biomechanical field as a cancellous bone surrogate, several works have been conducted over the last years to characterize this kind of structures [4, 8, 9]. Some of them deal with commercial foams [2, 4, 9–12] while others produce their own foams resembling cancellous bone [1, 8]. Among them, Szivek et al. [8] performed uniaxial compression tests of four mixtures of porous polyurethane foams. The mechanical properties obtained from the tests fell all within the range of those of human trabecular bone. Patel et al. [9] calculated the compressive properties of open cell PUR foams aiming at mimicking osteoporotic human cancellous bone ones, which was achieved only in terms of fracture stress. Further, Thompson et al. [13] studied also the shear properties experimentally and pointed out that to mimic cancellous bone behavior, anisotropy must be also considered.

Other studies have addressed fracture properties in PUR foams experimentally by three-point bending testing of notched specimens [14–16]. Some of these include numerical modelling of the crack evolution [14, 15], or use digital image correlation (DIC) technique [14, 16, 17]. The numerical models developed by Marsavina et al. [15] considered a homogeneous material and XFEM to model crack propagation under mixed mode testing conditions. The authors highlighted the importance of experimental validation (or calibration) of the numerical model, which in their case depended on several parameters.

DIC is an optical non-contact displacement measurement technique [18] preferable for cases where it is difficult to attach other measurement systems. It permits to estimate surface displacements and strains based on image pattern analysis and, in case of foams, microstructure may act as the grid (speckle) to be used for displacement estimation [19, 20]. Some authors have applied DIC to foamed structures [14, 16, 17, 20]. Among them, Jin et al. [16] applied DIC to closed-cell PUR foams and compared the heterogeneous strain estimations to finite element results, which were similar in a qualitative way. On the other hand, Chiang et al. [17] analyzed specimen size influence on the stress-strain response using a multi-speckle technique.

Although the deformation was almost uniform along the largest samples, the micro-size ones revealed heterogeneous patterns [17]. However, little work has been carried out in the literature regarding strain inhomogeneities analysis and fracture on foamed specimens under axial loading conditions [20, 21].

In foamed structures, microarchitecture has a major influence on the elastic and fracture properties [4, 7]. The advances on imaging systems have motivated studies accounting for an accurate morphological description. For example, Gómez et al. [10] analyzed the morphometry of two grades of open cell PUR foams by SEM and micro-CT and stated that 0.09 and 0.12 g/cm^3 foams have similar microstructural characteristics than osteoporotic human cancellous bone. Other previous works in the literature have developed finite element models of PUR foams from CT images [1, 4, 11, 12]. Some of them have applied micro-CT during specimen testing, which provides information about the deformation state at each load increment that can be used to validate finite element models [1, 11]. Special care must be taken when modeling is based on high resolution images, because both the characteristic structure parameters and the mechanical properties of the foam may be altered by the micro-CT setting parameters, resolution and the subsequent segmentation method applied [11, 22].

Some of the works in the literature dealing with commercial open cell polyurethane foams refer their results to the average properties provided by the manufacturer [4, 10]. Jonhson and Keller [4] pointed out significant differences between their elastic metrics and the values reported in the literature, which confirms the importance of accurate definition of testing conditions to make the results comparable. Since open cell polyurethane foams are often used to evaluate implant stability and local variations of microstructure are relevant to the pull-out strength predictions, finite element (FE) models based on high resolution images can help to get insight into the failure mechanisms of this kind of structures. Therefore, a thorough investigation of the influence of foam microarchitecture on its elastic and fracture behavior is relevant for implant design and failure mechanisms studies at the micro scale.

In this work, we aim at characterizing open-cell rigid polyurethane foams of three different densities from mechanical and morphometric perspectives. The mechanical characterization is conducted experimentally, through compression testing combined with the application of DIC to estimate full-field surface displacements and to describe compression fracture patterns. On the other hand, FE models developed from micro-CT images of some of the tested samples are generated and simulated under the experimental loading conditions, which enables the estimation of elastic and failure parameters to be used for numerical modeling. In addition, a morphometric analysis is performed, which is then related to the mechanical properties of the samples. The detailed information about morphometry, elastic constants and strength limits provided in this work can be useful for researchers and practitioners that make use of these polyurethane foams in orthopedic implants and cement augmentation evaluations.

2. Materials and methods

2.1. Description of specimens: Open cell polyurethane foams

Three different density grades of open-cell polyurethane foams (Sawbones, Sweden) are analyzed in this study, Fig. 1. The grades are denoted as follows: Low density foam (LD, Ref. #1522-507), medium density foam (MD, Ref. #1522-524) and high density foam (HD, Ref. #1522-525) [23]. Each foam grade is sold in a block of 13x18x4 cm, from which a series of specimens are machined. The manufacturer provides some mechanical and morphological properties for each foam grade, like the apparent compressive Young's modulus (E_{app}), the compressive strength (σ_{f}) and foam volume fraction (FV/TV). The structure is over 95% open cell and the cell size is between 1.5 to 2.5 mm. The manufacturer acknowledges a wide scattering on the mechanical properties, but they report average properties of each foam grade blocks, summarized in Table 1.

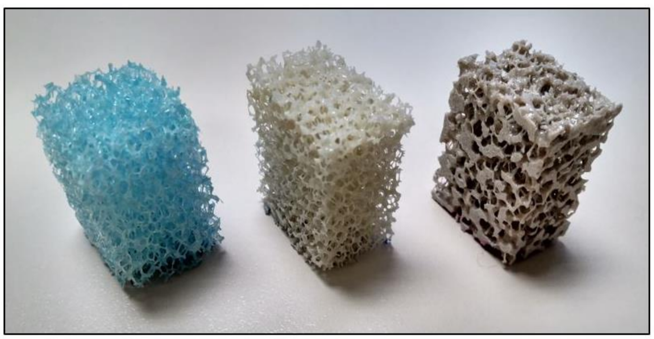

Figure 1: Specimens of different apparent densities analyzed in this work: low density foam (LD) (left), medium density foam (MD) (centre) and high density foam (HD) (right).

Table 1: Mechanical and morphological properties provided by the manufacturer for each open cell graded foam from [23].

Foam grade	Density [g/cm^3]	FV/TV [%]	σ_{f} [MPa]	E_{app} [MPa]
# LD	0.12	10.6	0.28	18.6
# MD	0.24	15.4	0.67	53
# HD	0.48	30.8	3.20	270

2.2. Preparation of specimens

A series of parallelepiped specimens (total of 30, 10 of each density grade) were extracted from the initial open-cell polyurethane foam blocks. The specimens were chosen to maintain the initial block thickness and to have a quadrilateral base, Fig. 1. The average specimen dimensions are 25 mm base-side and 40 mm height. The foam blocks were machined using a table saw, with constant water irrigation and low advance velocity to reduce the cutting effects. In any case, the disruption of the reticular microstructure due to specimen machining has a relevant effect on the mechanical properties as it happens for cancellous bone [24–26]. In case of cancellous bone, a reduction from 20 to 50 % on the apparent modulus has been reported due to the so-called side artifacts, and a similar effect may be expected for other foamed structures.

Table 2: Mean and standard deviation of the apparent density (ρ_{app}) measured for each density grade.

Foam grade	ρ_{app} [g/cm^3]
LD	0.107 ± 0.009
MD	0.239 ± 0.017
HD	0.442 ± 0.022

In addition, special attention was taken to maintain parallel faces at each specimen to avoid point loads and stress concentration during compression testing due to uneven surfaces. Each specimen was weighted and the apparent volume was estimated, which allows to estimate the apparent density, summarized in Table 2. It can be noted that foam blocks heterogeneity and specimen machining result in a slightly apparent density reduction compared to the values reported by the manufacturer in Table 1. Testing directions were defined as follows, see Fig. 2 top: 1 (or axial) is the initial foam block depth direction, while 2 and 3 are the transverse directions.

2.3. Micro-CT scanning and segmentation

Six specimens (two of each density) were scanned using a micro-CT (V|Tome|X s 240, GE Sensing and Inspection Technologies) through the CENIEH (Burgos, Spain) micro-CT service, with an isotropic voxel resolution of 24 μm (voltage 80 kV, intensity 200 μm, integration time 200 ms). Then, the micro-CT images were segmented using ScanIp software (Simpleware, UK), following a manual image thresholding method combined with mask connectivity analysis, Fig. 2 bottom. In Fig. 2 top, a 3D reconstruction of the three grades of foam samples generated from micro-CT images is shown. The resulting 3D segmented masks were analyzed to estimate morphometric parameters in the next section.

2.4. Morphometric characterization

In order to characterize the microstructure of the different open cell foam specimens, a morphometric analysis of the segmented masks was carried out. We define the following parameters: foam volume fraction (FV/TV), foam surface area to total volume ratio (FS/TV), foam surface area to material (PUR) volume ratio (FS/FV), mean strut thickness (Str.Th), mean void dimension or mean strut separation (Str.Sp), strut number (Str.N), fractal dimension (D_{3D}), degree of anisotropy based on mean intercept length (DA_{MIL}) and connectivity density (Conn.D). These parameters are commonly used for cancellous bone microstructure characterization [20, 33].

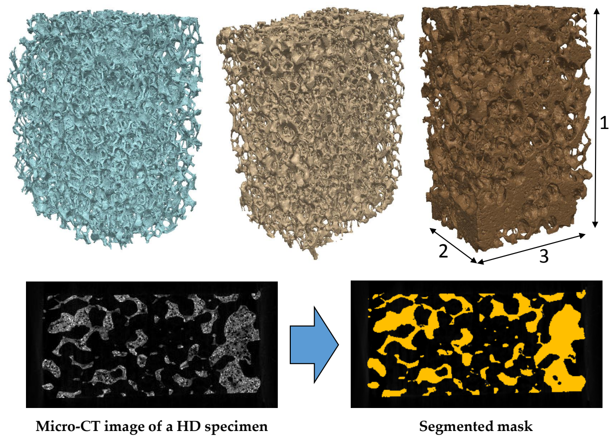

Figure 2: 3D reconstruction of each foam grade generated from micro-CT images: LD (top left), MD (top centre) and HD (top right). Testing directions are defined as 1 (axial) and 2,3 (transverse). Segmentation of a micro-CT image of a HD specimen through a manual thresholding approach (bottom).

We remark that these parameters are average measurements for each region of interest. Having further information of the foam morphology is important for the study of local effects in the structure as in case of damage, fracture, screw insertion or cement augmentation. To give insight into the variation of those morphometric parameters, we also calculated them in slices of about 5 mm of thickness along specimen height.

2.5. Experimental characterization

We performed mechanical non-destructive compression tests to estimate the apparent Young's modulus ($E_{\mathrm{app,i}}$) of the different graded foams in their 3 main directions (i=1,2,3 or axial(ax)/transvers(trans)) and destructive compression tests to characterize fracture behavior in the axial direction. In addition, we applied DIC to images acquired during testing in order to analyze the inhomogeneous strain distribution at failure.

2.5.1. Compression tests

Quasi-static compression tests were conducted following this protocol: A 10 N pre-load was defined; then, after 5 preconditioning cycles, an increasing load was applied with a displacement rate of 1 mm/min between 0.5 % and 1 % strain levels to avoid damage in the specimens.

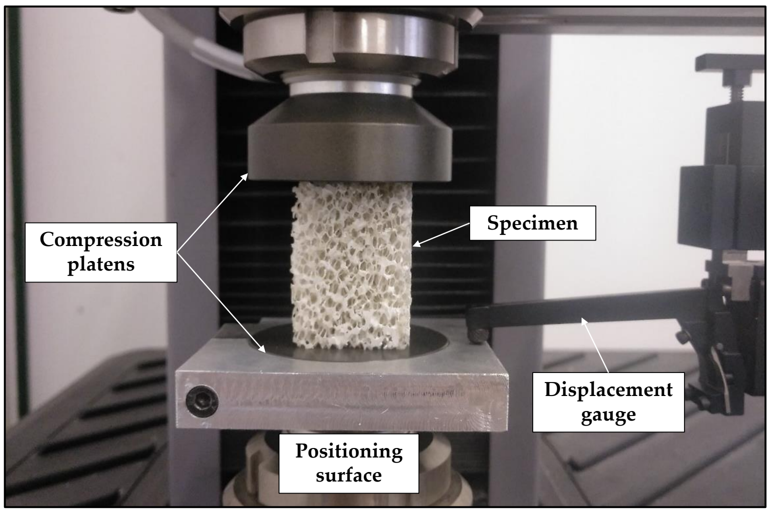

Figure 3: Testing set up for compression of foam samples. A local displacement gauge is used to measure the displacement between compression platens so as to avoid any compliance effect of the load chain.

Tests were carried out using an electromechanical testing machine (MTS Criterion C42), with aluminum compression platens (MTS ref.: FYA502A) for the compression tests and measuring the displacement between compression platens using a displacement gauge (MTS ref.:632.06H-20). The apparent stiffness ($E_{\mathrm{app,i}}$) of each specimen in its 3 main directions was determined from the linear response after the last preconditioning cycle, while failure stress (σ_{f}) was defined as the peak value following the elastic response and the failure strain (ε_{f}) was defined as the strain at σ_{f}. Yield stress (σ_{y}) and strain (ε_{y}) were estimated through the 0.2% convention. The compression test rig is shown in Fig. 3.

2.5.2. Full-field displacement measurement using Digital Image Correlation (DIC)

The objective of the DIC analysis is to characterize the strain field distribution over specimen frontal surface and detect compression fracture patterns from a speckle and non-speckle approaches. The strain field distribution and failure pattern results will be used to validate the finite element models predictions and the failure model proposed.

We used VIC-2D Digital Image Correlation software (v.6.0.2 Correlated Solutions Inc., US), a high resolution fixed focal lens (HF7518V-2, Myutron, Japan) with 12 Mpx resolution, extension rings (10 mm), 65 mm focal length and a spotlight. Perpendicular camera-specimen relative position was ensured to avoid out-of plane displacements during testing. To evaluate the use of speckle, half of the specimens scanned by micro-CT (3) were speckled, which consisted of the application of a white spray paint coat followed by a black spray paint speckle to increase contrast. The other half were analyzed benefiting from the irregularities of the microstructure.

We used a normalized squared differences (NSSD) pattern matching criterion and an incremental correlation, where each image is compared with the previous one instead of the reference image. A high sub-pixel accuracy was ensured using a high order interpolation spline method (8-tap). A squared facet (the grid in which ROI is divided) of 81 mm pixels size, a step size of 5 pixels and a strain filter size of 21 pixels were defined for the strain field calculation. Those parameters were defined based on noise minimization and failure pattern localization accuracy.

2.6. Finite element modeling

We developed finite element models based on high resolution micro-CT to reproduce the elastic and fracture behavior of the open cell foam specimens registered in the experiments. Then, the elastic and failure properties for each specimen are estimated by inverse analysis using the experimental force-displacement curve. Finite element meshes were generated from the micro-CT segmented masks using ScanIp (Simpleware, UK). The models were meshed with linear tetrahedral elements (coded C3D4 in Abaqus), resulting in finite element models of about 3 million elements and one million nodes for LD and MD grades and about 6 million elements and 1.5 million nodes for HD grade.

The finite element models generated using Abaqus (6.14, Dassault Systems, US) for each specimen are shown in Fig. 4. Linear-elastic isotropic material properties were assigned in the simulations, calibrated using the experimental data. A Poisson's ratio of 0.3 was assumed from the literature [11]. Boundary conditions were defined to mimic the experimental tests, imposing the displacement registered in the experiments on top face nodes and constraining the displacements in the load direction on the bottom surface. Lateral surfaces are free (unconfined compression).

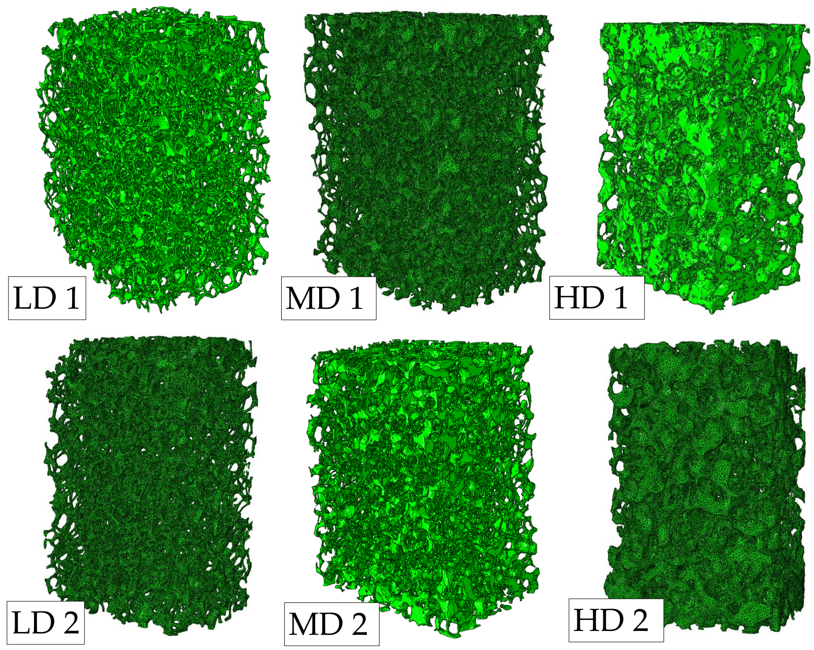

Figure 4: Finite element models developed for the six specimens scanned using micro-CT: LD (left), MD (centre) and HD (right). Three of the 3D rendered foams show the finite element mesh (one for each grade).

2.7. Compression failure modeling

In this study, we consider that foam failure at the strut level occurs in two phases: first the stiffness is reduced in the damage phase, following a continuum damage approach, and then the complete fracture of the struts is modeled using the element deletion technique. This approach has been used to model compression fracture in foam-like structures as cancellous bone [20, 27]. These damage and fracture approaches were implemented using an Abaqus user's subroutine (USDFLD).

In the quasi-static regime, the isotropic relation of elasticity under damage mechanics approach is expressed by Eq. 1 [28]:

$$\sigma_{ij} = (1 - D)C_{ijkl}\varepsilon_{kl} \tag{1}$$

where D is the damage variable, σ_{ij}, ε_{kl} are the stress and strain tensors and C_{ijkl} is the constitutive elastic tensor. We propose D to vary following an isotropic damage law experimentally fitted (Eq. 2) for cancellous bone based on an equivalent strain (Eq. 3), because of its similarity to foam structure [20, 27]. Material properties are reduced from compression yield strain ($\varepsilon_{\mathrm{y,c}}$) until its 5 % at $\varepsilon_{\mathrm{f,c}}$. At this point, the finite element is deleted.

$$D = \begin{cases} 0 & \varepsilon_{\mathrm{eq}} \leq \varepsilon_{\mathrm{y,c}} \\ 0.95(\frac{\varepsilon_{\mathrm{eq}}}{\varepsilon_{\mathrm{f,c}}})^2 & \varepsilon_{\mathrm{y,c}} < \varepsilon_{\mathrm{eq}} < \varepsilon_{\mathrm{f,c}} \\ 0.95 & \varepsilon_{\mathrm{eq}} \geq \varepsilon_{\mathrm{f,c}} \end{cases} \tag{2}$$

$$\varepsilon_{\mathrm{eq}} = \sqrt{\frac{2}{3}\varepsilon_{ij}\varepsilon_{ij}} \tag{3}$$

The yield strain ($\varepsilon_{\mathrm{y,c}}$) and ultimate strain ($\varepsilon_{\mathrm{f,c}}$) parameters need to be back calculated from the simulation, so this approach enables the estimation of failure strains.

3. Results and discussion

3.1. Stress-strain relationships from quasi-static compression tests

After the five preconditioning cycles, the stress-strain response registered for three foam densities may be divided in an approximately linear part, followed by a non-linear stiffness decrease until the ultimate point, Fig. 5. Then, a softening region is observed within post-yielding until material stacks and the load bearing capacity increases (not shown in Fig. 5). The preconditioning cycles effect is clearly seen as a significant difference between the initial slope and the one after the cycles, helping to reduce the side artifacts [26].

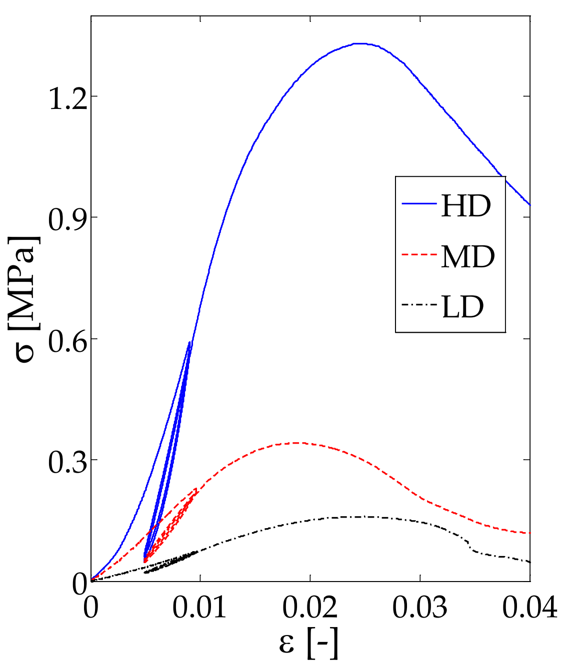

Figure 5: Stress-strain response registered in compression tests for three specimens of different densities.

3.1.1. Apparent Young's modulus

Compressive stiffness results along the axial and transverse directions are summarized in Table 3. For the HD grade, the transverse direction is stiffer than the axial one, while for the MD and LD grades the axial direction is stiffer. The morphometric analysis along specimens height (section 3.2) reveal that, for HD specimens, the material distribution is not homogeneous and more material is placed near the upper and bottom surfaces. In those volumes, the foam volume fraction is around 40%, while in the center of the specimens it decreases to around 20%. Therefore, when the samples are compressed in the axial direction, the central part of the specimens is more compliant and governs the overall behavior (springs in series effect). In the transverse direction there is more material that stiffens the elastic behavior (springs in parallel effect). In case of MD and LD specimens, the variation of the foam volume fraction along the specimens is lower (from 20% to 12% and from 12% to 8 %, respectively) and specimens behave more isotropically.

Table 3: Mean and standard deviation (SD) values of compressive stiffness for each foam grade in their axial and transverse directions and yield and fracture stresses and strains measured through destructive testing in the axial direction.

	$E_{\mathrm{app,ax}} \pm$ SD [MPa]	$E_{\mathrm{app,trans}} \pm$ SD [MPa]	σ_{y} [MPa]	ε_{y} [%]	σ_{f} [MPa]	ε_{f} [%]
HD	108.37±27.04	160.56±63.65	1.00 ± 0.28	1.5 ± 0.2	1.09 ± 0.32	1.9 ± 0.3
MD	32.59±4.45	29.45±12.03	0.34 ± 0.05	1.6 ± 0.2	0.38 ± 0.06	2.1 ± 0.3
LD	8.94±1.2	6.14±1.75	0.11 ± 0.02	1.8 ± 0.1	0.13 ± 0.02	2.5 ± 0.2

For the HD specimens, the apparent modulus has an average value of 108 MPa for the axial direction and 161 MPa for the transverse direction. MD and LD samples present less scatter than HD. In case of MD foams, we found a mean value of 33 MPa for the axial direction and 29.5 MPa for the transverse one, whereas for LD group, the axial direction has a mean apparent modulus of 9 MPa and the transverse one of 6 MPa.

The manufacturer reports stiffness values for each foam grade (Table 1), but the testing conditions, directions or the standard deviation of the values provided are not specified in the catalog. For each foam density, the reported values are significantly greater than our measurements. After querying the manufacturer for further details about the testing protocol and results, they confirmed that specimen dimensions are similar to the ones in this work but their measurement system is global instead of local. The manufacturer observed a wide scattering of the results, not reported in the catalog. In addition, specimen machining may also be responsible for some of the scattering in the mechanical properties due to side artifacts resulting from connectivity disruption.

Other works in the literature have provided stiffness values very similar to our measurements. Johnson and Keller [4] studied the static and dynamic behavior of LD samples from Sawbones and reported a stiffness value in the axial direction of approximately 6 MPa, three-fold less than the manufacturer value, which is similar to our measurements. However, they associate the differences to specimen dimensions and hypothesize that the manufacturer tested the whole foam blocks.

3.1.2. Yield and ultimate stresses and strains

The estimation of yield and ultimate properties for each specimen is given in Table 3. The HD group presents a mean yield stress of 1 MPa and a mean ultimate stress of 1.09 MPa. The latter is about one third of the value (3.2 MPa) reported by the manufacturer. On the other hand, a mean yield strain of 1.5 % and a mean ultimate strain of 1.9 % were measured for HD specimens. The MD group presents mean values for the yield and ultimate stresses of 0.34 and 0.38 MPa, respectively, which are about half the value reported by Sawbones. As happened to the HD group, the yield strain values tend to concentrate around 1.6 %, while the ultimate strain are about 2.1 %. Similarly, approximately half the reported values by the manufacturer were measured for the LD ultimate stresses (0.127 MPa) and a mean yield stress of 0.111 MPa, as summarized in Table 3. In this case, a mean yield strain of 1.8 % and a mean ultimate strain of 2.5 % were measured.

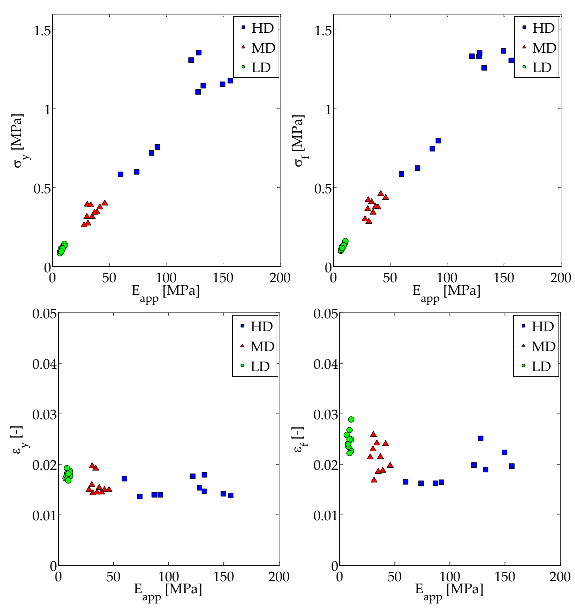

Figure 6: Representation of the yield and ultimate stresses (σ_{y} and σ_{f}) (top) and the yield and failure strain (ε_{y} and ε_{f}) (bottom) as a function of the apparent modulus ($\mathrm{E}_{\mathrm{app}}$) for the three foam grades.

Yield and ultimate stresses show a linear relationship with the apparent modulus, see Fig. 6. Other authors, like Fürst et al. [1] reported similar linear relationships between ultimate stress and modulus. In this sense, the open cell foams resemble cancellous bone strength-modulus dependence, which has been the reported in the literature [29]. From our results, this linear relationship is σ_{y}=0.008332 $\mathrm{E}_{\mathrm{app}}$+0.04376, with a correlation coefficient (R^2) of 0.967. The following linear expression was found between ultimate stress and modulus: σ_{f}=0.009079 $\mathrm{E}_{\mathrm{app}}$+0.04947, ($R^2$=0.98).

Yield strain values show little scattering and they seem to be less dependent on microstructure and govern the failure process. The plot reveals that yielding is relatively constant in terms of strain for a wide range of densities, see Fig. 6. These results suggest that strains may control failure of open cell polyurethane foams, as it happens for cancellous bone [29–31]. In the case of ultimate strain (ε_{f}), a larger scatter is found, with an incremental difference of 30 % between LD and HD groups, Fig. 6. The wide scatter of ultimate strain values has been also reported in the literature for cancellous bone [31, 32]. However, a small but significant dependence on volume fraction or microstructure may exist because yield and ultimate strains increase with decreasing density.

3.2. Morphometric characterization results

Table 4 shows the morphometric parameters for the 6 specimens scanned by micro-CT, two for each foam grade. The first conclusion is that each foam grade is characterized by several parameters, except for Str.Sp, Str.N and $\mathrm{DA}_{\mathrm{MIL}}$, whose values are similar for all foam grades. Our estimations of the mean strut separation (Str.Sp) are in the upper range of the manufacturer values (mean cell size between 1.5 and 2.5 mm) for all the foam densities.

MD samples show the lowest Str.Sp value (2.16 mm), followed by HD (2.36 mm) and LD (2.45 mm).

Table 4: Morphometric parameter results for each open cell polyurethane foamed specimen.

Sample	FV/TV [%]	FS/TV [mm^{-1}]	FS/FV [mm^{-1}]	Str.Th [mm]	Str.Sp [mm]	Str.N [mm^{-1}]	D_{3D} [-]	DA_{MIL} [-]	Conn.D [mm^{-3}]
HD1	30.83	1.08	3.61	1.82	2.38	0.169	2.73	1.11	0.059
HD2	30.81	1.20	3.89	1.81	2.34	0.171	2.72	1.10	0.093
MD1	15.40	0.93	6.04	0.69	2.15	0.223	2.56	1.13	0.212
MD2	15.39	0.89	5.77	0.73	2.17	0.210	2.58	1.11	0.168
LD1	8.01	0.83	10.35	0.34	2.34	0.234	2.45	1.15	0.507
LD2	10.60	0.86	8.07	0.51	2.57	0.208	2.49	1.12	0.240

HD specimens show the highest Str.Th value, 1.8 mm, which decreases to 0.7 mm for MD and about 0.4 mm for LD specimens. Regarding strut number (Str.N), lower differences between foam grades have been found: a 27% difference between HD and MD, while only a 2% difference between MD and LD. The degree of anisotropy values reveal the existence of a preferred orientation but of a low degree ($DA_{MIL} \simeq 1.1$). This is indicative of a transversely isotropic mechanical behavior, containing a direction of higher stiffness. On the other hand, connectivity density values (Conn.D) increase for decreasing foam density, and it is related to the amount of material in the region of analysis. Therefore, HD foams present a lower number of connections compared to MD and LD foams because denser foams have more material but less connected, see Fig. 2.

The morphometric results estimated for subvolumes of approximately 5 mm height for the six specimens scanned by micro-CT are depicted in

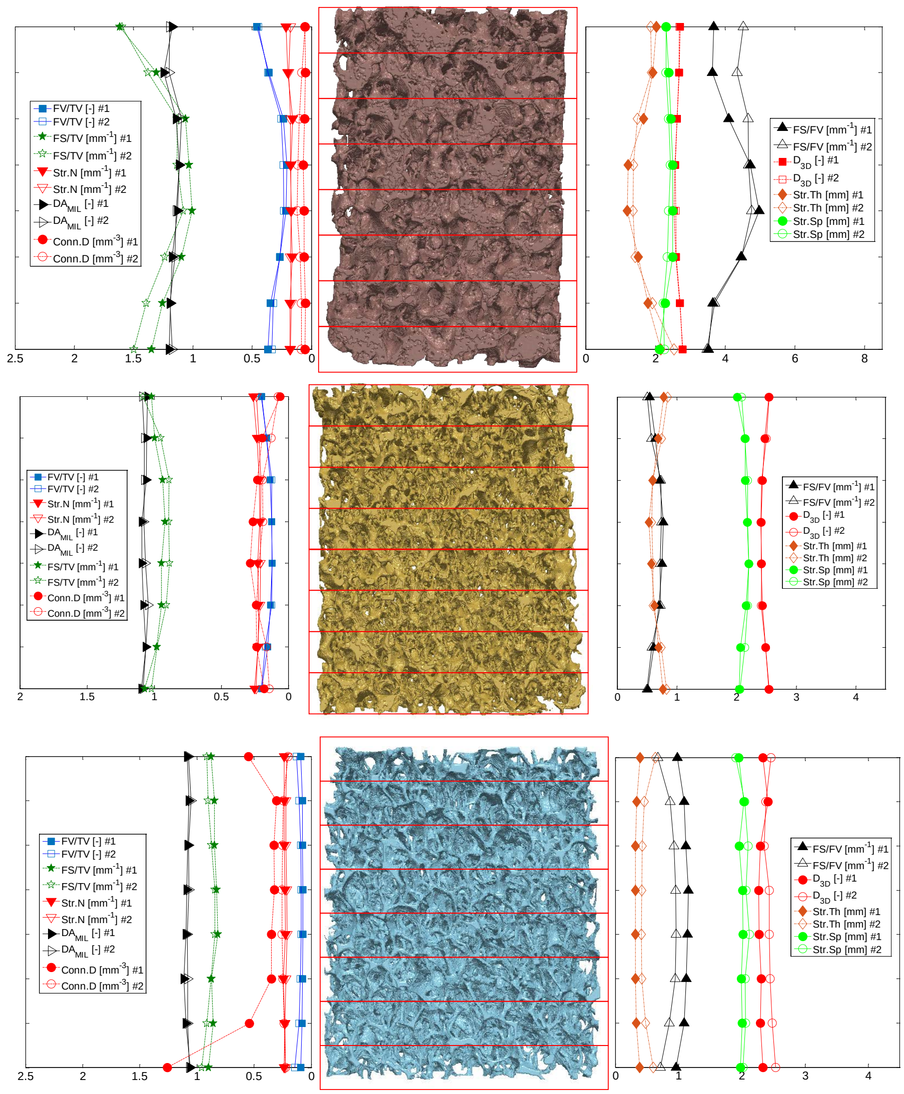

Figure 7: Results of the morphometric analysis along specimen thickness: HD (top), MD (middle) and LD (bottom) specimen thickness. For each subvolume, marked with red boxes, the parameters that define the microstructure were estimated after averaging in each subvolume.

Fig. 7. HD results show a greater concentration of material in the upper (FV/TV = 45 %) and bottom surfaces (FV/TV = 34 %), while in the central volume presents a lower volume fraction (FV/TV = 20 %). The relationship between the surface area and the total volume (FS/TV) shows the same trend with the lowest values in the mid-region of the sample (1-1.2 mm^{-1}) with increasing values at the surfaces (1.3-1.6 mm^{-1}). The opposite trend is found when considering the material (PUR) volume as a reference (FS/FV) instead of the total volume: the highest values in the center (5mm^{-1}) while the lowest near the surfaces (3.5mm^{-1}). The mean strut thickness (Str.Th) variation is in line to the foam volume fraction, the greatest values on the surfaces (1.9-2.5 mm) and the lowest in the middle of the specimen (1.2-1.4 mm). In contrast, a mean void size of between 2.1 and 2.3 mm near the surfaces increases up to 2.5 mm in the center. Other parameters, such as the anisotropy degree, Str.N, D_{3D} and the connectivity density are quite homogeneous within the foam, see Fig. 7.

As regards the MD specimens, FV/TV, FS/TV and FS/FV present an analogous behavior to HD specimens, but with less variation. For example, foam volume fraction changes from 20% to approximately 12%. DA_{MIL} and fractal dimension show little variation along the sections: 3.8% for the anisotropy, and about 5% for the fractal dimension. The mean strut thickness increases from 0.55 mm in the central section to 0.8 mm in the external sections. On the contrary, the mean void dimension takes a 2.2 mm value in the center while around 2.05 mm at the surfaces. Regarding connectivity density, the values estimated are higher than for HD specimens, which indicate that more connections per unit volume are found for MD specimens.

The morphometry of the LD foams, resembling osteoporotic cancellous bone, is more homogeneous in terms of FV/TV, FS/TV, and FS/FV values, compared to the other foam grades, see Fig. 7. For example, volume fraction changes from 7-8.8 % to 9-12.8% near the surfaces. Again, parameters like Str.N, DA_{MIL} and D_{3D} show little variation in the section analysis. The connectivity density values are greater than for MD and HD foams, and present intra-specimen variation because higher values are found for specimen LD1, the one of lower FV/TV. For the specimen LD1, Str.Th varies from 0.31 mm in the central sections to 0.39 in the external ones, while for LD2, greater values are found: 0.41 mm and 0.63 mm, respectively. In this low apparent density foams, the mean void dimension is more constant along the sections than for MD and HD specimens, see Fig. 7.

3.3. Relationships between microstructural parameters defining cancellous bone specimens and experimental compression tests

We have calculated linear relationships between the morphometry (FV/TV, FS/TV, FS/FV, Str.Th, Str.Sp, Str.N, D_{3D}, DA_{MIL} and Conn.D) and mechanical response (E_{app}, σ_y, σ_f, ε_y and ε_f). The correlation coefficients (R^2) of the morpho-mechano linear regressions are summarized in Table 5. Some morphometric parameters show a high degree of correlation to the mechanical response (E_{app}, σ_y, σ_f and ε_y), such as FV/TV, FS/TV, Str.Th, Str.N and D_{3D}. Other parameters (DA_{MIL}, FS/FV and Conn.D) present a lower but significant degree of correlation, while mean void dimension (Str.Sp) shows no correlation to any of the mechanical variables. In addition, fracture strain (ε_f) does not correlate to morphometry. This lack of correlation is also found in cancellous bone morpho-mechano dependencies.

Table 5: Correlation coefficients (R^2) of linear regression between morphometry and mechanical response parameters. Values of R^2 greater than 0.9 are typed in bold.

	σ_y	ε_y	σ_f	ε_f	E_{app}
FV/TV	**0.989**	**0.963**	**0.990**	0.496	**0.969**
FS/TV	**0.924**	0.836	**0.927**	0.431	**0.953**
FS/FV	0.786	0.771	0.779	0.402	0.727
Str.Th	**0.985**	**0.975**	**0.986**	0.531	**0.977**
Str.Sp	0.004	0.002	0.003	0.051	0.001
Str.N	0.850	**0.925**	0.843	0.690	0.864
D_{3D}	**0.964**	**0.949**	**0.959**	0.510	**0.927**
DA_{MIL}	0.535	0.610	0.513	0.697	0.549
Conn.D	0.595	0.634	0.586	0.417	0.549

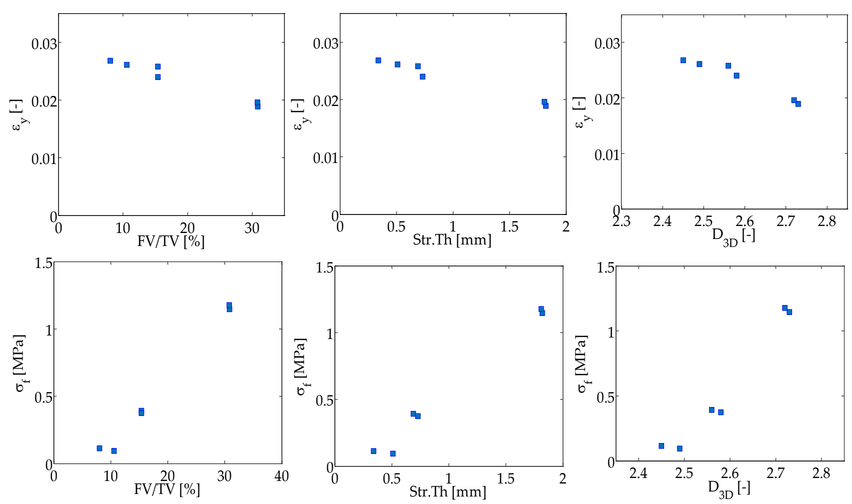

Figure 8: Some of the most significant relationships between morphometric parameters and yield strain and failure stress.

Fig. 8 shows some of the linear regressions with high R^2 between morphometry and ultimate stress. These results evidence in a quantitative way the fact that microstructure controls the mechanical response of open cell foams of different densities. Other authors have investigated relationships between morphometry and mechanical properties for this type of structures [1]. Some of the reported relationships are in line with our observations, like is the case of FV/TV, Tb.N or a weak correlation of Conn.D with modulus or strength. Other parameters that showed correlation in our results did not correlate to mechanical parameters in [1]. On the other hand, the morphometric parameters that explain a variation in the mechanical properties of our foam specimens match the ones of cancellous bone [20, 29, 33]. For example, volume fraction, surface area to volume ratio, mean strut thickness and fractal dimension presented a significant correlation to the apparent modulus and the failure stresses [20, 29, 33]. Moreover, a lack of correlation between microstructure and the ultimate strain has been also found for cancellous bone [20, 29].

3.4. Finite element modeling results

3.4.1. Elastic modulus and failure properties estimation through FEM and testing

Table 6 shows the tissue Young's modulus (E_i) estimated for each specimen by inverse analysis using FEM and calibration with test results. The values estimated for the elastic modulus present differences according to the foam grade. A mean elastic modulus of 3 GPa was estimated for the material in high density foams, 2.7 GPa for the medium density foams and 1 GPa for the low density foams. This could be expected because in the manufacturer's catalog it is said that the material is a composite foam made of urethanes, epoxies and structural fillers, and the material composition may be different for each foam grade.

Table 6: Young's modulus (E_i), yield (ε_y) and fracture strains (ε_f) calculated for each specimen using finite elements after calibration with the experimental force-displacement curve.

	E_i[GPa]	ε_y [-]	ε_f [-]
HD1	3.290	0.050	0.070
HD2	2.809	0.040	0.058
MD1	2.119	0.03	0.070
MD2	3.358	0.03	0.070
LD1	1.543	0.0225	0.048
LD2	0.579	0.04	0.0775

The results of the back calculation of yield and failure strains for each specimen using experiments and finite element models are summarized in Table 6. The failure strain values obtained are quite homogeneous for each density grade and also between MD and LD groups. HD foams present a mean yield strain of 0.045, 0.03 for MD and 0.031 for LD. The slightly higher value reported for HD specimens may be related to its different composition, as it may contain more structural fillers. On the other hand, fracture strains were also considerably homogeneous between samples and density grades, as shown in Table 6. A mean ultimate strain of 0.064 was estimated for the HD group, 0.07 for MD and 0.063 for LD specimens. Therefore, despite different density and microstructure, tissue yield and ultimate strains are relatively constant for the 6 samples analyzed.

The numerical models reproduce the elastic response and predict the failure load, see Fig. 9. However, a slight load overestimation is observed prior to the ultimate point. Nevertheless, it is shown with the numerical models that the equivalent strain governs failure of the foamed structures and it describes with high accuracy the compression response and the fracture pattern observed experimentally.

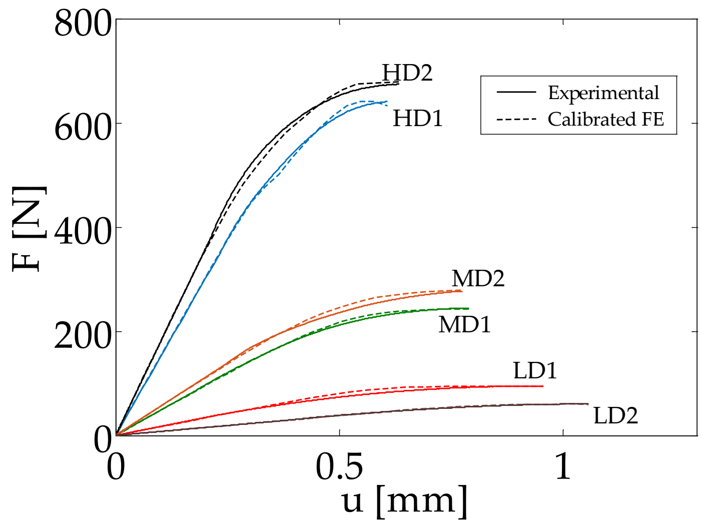

Figure 9: Comparison of the force-displacement curve obtained from experiments and simulations.

3.5. Fracture patterns characterization using finite elements and DIC

In Fig. 10, we compare the equivalent strain field obtained through the application of DIC to images taken during compression testing and the finite element predictions. Failure appeared at localized zones and dominated by microarchitecture. DIC detects strain inhomogeneities and clearly localizes failure at the apparent level, while FEM results are more localized and sometimes present more difficulties to visualize failure patterns. Half of the specimens (HD1, MD1 and LD1) were speckled, while the rest used their morphology to calculate the displacement field. The use of a speckle shows little influence on the failure pattern detection. Therefore, microstructure has enough pattern to perform the displacement correlation, see Fig. 10.

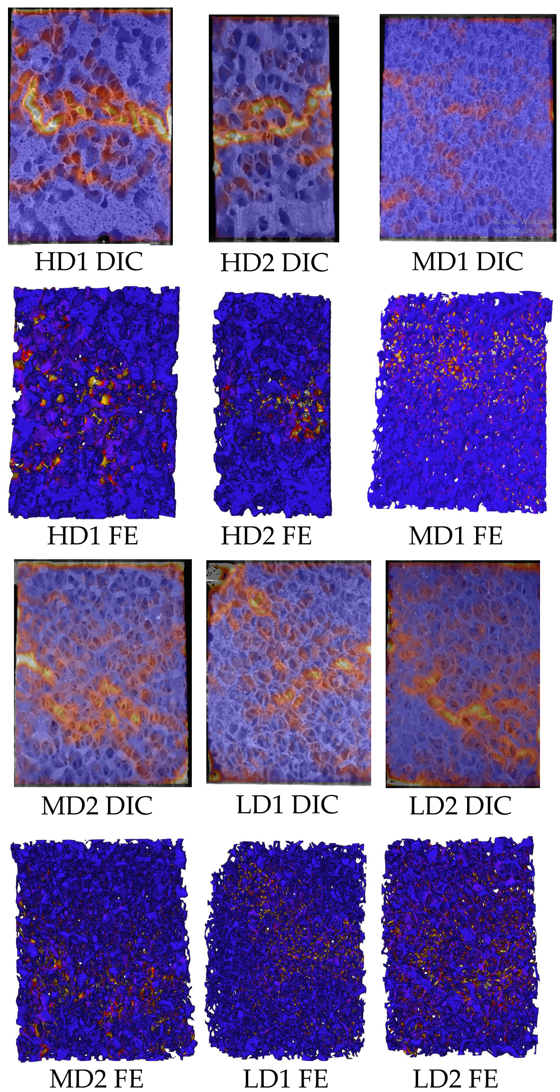

Figure 10: Representation of equivalent strain field using DIC and FE results. Cold colors represent low equivalent strains, while warm colors high equivalent strain values.

High density foams exhibit a failure pattern concentrated in the central region of the specimens, with a match between DIC and numerical predictions, even for the secondary fracture patterns, see Fig. 10. On the other hand, medium density specimens present a main fracture in the central part of the specimen and other secondary inclined failure patterns detected by DIC and also predicted by the finite element models, Fig. 10. However, some failed regions in the upper part of MD1 appear in the simulations and the failure pattern is more difficult to distinguish in the models, see Fig. 10. Nevertheless, similarities can be observed between DIC and FE simulations. An inclined failure pattern is detected by DIC and also predicted by the numerical model.

Specimen LD1 and LD2 present some inclined fracture planes. These are maximum shear planes at 45^{o} with respect to the applied compressive load. It can be noted that volume fraction has an influence on the fracture shape. In our results, the high density foams showed a flat central fracture area, while medium and low density specimens presented more inclined fracture patterns due to planes of maximum shear.

The application of DIC to detect compression failure patterns in open cell polyurethane foams has allowed the validation of our FE models to predict failure response. Our model accurately predicts the failed regions observed experimentally and supports the idea that failure in foams is controlled by strains.

4. Limitations of the study

We acknowledge some limitations of the study. First, specimen preparation involves machining, which induces a disruption of the microstructural lattice and influences the mechanical characterization. Therefore, an analysis about machining influence on mechanical performance should be addressed in order to elucidate whether the variability observed in the elastic and failure properties is due to specimen-specific variations or it is result of the specimen preparation. On the other hand, the approach we used to estimate elastic and failure properties combining FEM and experiments is conditioned by the latter so, if any artifact influenced the measurements it also did into the back calculated elastic and failure properties. As regards the relationships between microstructure and mechanical behavior, our study involves only 6 specimens (2 of each density) so the regressions obtained should be confirmed in larger datasets.

5. Conclusions

In this work, we have characterized open cell polyurethane foams of three different densities from morphometric and mechanical perspectives. The morphometric characterization was performed on 6 specimens scanned by micro-CT. The study of slices of 5 mm thickness revealed different morphometry evolution across the sample thickness according to density. The inhomogeneities were higher for the high density (HD) foams, which concentrate more material near the top and bottom surfaces. Morphometry varied according to that material distribution: for example, a lower volume fraction, foam surface to volume ratio or mean trabecular thickness were measured in the central region of HD samples. For some parameters, the inhomogeneities were high, like volume fraction, which varied from 40 % near the surfaces to about 20 % in the middle. Other parameters, like fractal dimension or connectivity density presented little changes within HD grade. MD foam grade is more homogeneous than HD, but presents similar trends about morphometry variation within a specimen, though of a much lower degree. In case of LD foam grade, the specimens are the most homogeneous. These analyses may be used to choose between cancellous bone surrogates according to the homogeneity needed for the experiments.

Moreover, the morphometry results of the whole specimens were used to analyze morpho-mechano dependencies through the calculation of linear regressions. Some parameters, like FV/TV, FS/FV, Str.Th, Str.N and D showed correlation to the elastic modulus, yield and ultimate stresses and yield strain measured in the experiments.

As regards the mechanical characterization, an orthotropic material behavior, close to transversely isotropic was found. In case of HD specimens, the lower material disposition in the central part makes the block thickness direction less stiffer than the transversal ones. In case of MD and LD specimens, the axial direction is stiffer than the transversal ones, but at a lower degree. A linear relationship between strength (yield stress and ultimate stress) and stiffness was captured from the experiments, so the stiffer a sample is, the higher the strength at failure. Yield strains (ε_{y}) were relatively constant (HD foams had a mean value of 1.5 %, MD 1.6 % and LD 1.8 %) and more scatter was found for the ultimate strain (ε_{f}) (mean values of 1.9 %, 2.1 % and 2.5 % for HD, MD and LD specimens).

As regards the numerical characterization of the compression failure behavior, a mean tissue Young's modulus of 3 GPa was estimated for HD, 2.7 GPa for MD and 1 GPa for the LD foams. The model detected the failure experimental pattern with high accuracy, which matched DIC failure prediction results. The use of a speckle had no significant influence on DIC failure pattern detection and microstructure has enough pattern to perform the displacement correlation. Yield and ultimate strains back-calculated combining experiments and finite element modeling led to values approximately constant over the density grades analyzed. HD specimens presented a higher yield strain (0.045) than MD and LD specimens (0.03), which may be related to the inclusion of more structural fillers in the high density group. The ultimate strain properties estimated showed little variation between samples, with a mean value close to 0.07.

The information provided in this work is relevant for a more accurate mechanical characterization needed in cement augmentation analyses or orthopedic implants assessment. The thorough morphometric analysis reported here provides information about its local variation and its relationship to mechanical behavior.

CRediT authorship contribution statement

Ricardo Belda: Conceptualization, Methodology, Software, Validation, Investigation, Data Curation, Writing - Original, Writing - Review & Editing, Visualization. **Marta Palomar:** Software, Formal analysis, Data Curation, Investigation, Validation, Writing - Original, Writing - Review & Editing, Visualization. **Miguel Marco:** Methodology, Formal analysis, Investigation, Writing - Original, Writing - Review & Editing. **Ana Vercher-Martínez:** Supervision, Project administration, Funding acquisition, Writing - Original, Writing - Review & Editing. **Eugenio Giner:** Conceptualization, Validation, Resources, Supervision, Project administration, Funding acquisition, Writing - Original, Writing - Review & Editing, Visualization.

Declaration of competing interest

The authors declare no competing interests.

Acknowledgments

This work was supported by the Spanish Ministerio de Ciencia, Innovación y Universidades grant numbers DPI2013-46641-R and DPI2017-89197-C2-2-R and the Generalitat Valenciana (Programme PROMETEO 2016/007). The micro-CT acquisitions were performed at CENIEH facilities with the collaboration of CENIEH staff.

References

[1] D. Fürst, S. Senck, M. Hollensteiner, B. Esterer, P. Augat, F. Eckstein, A. Schrempf, Characterization of synthetic foam structures used to manufacture artificial vertebral trabecular bone, Mat. Sci. Eng. C-Bio. S. 76 (2017), pp. 1103-11. http://dx.doi.org/10.1016/j.msec.2017.03.158

[2] T.L. Mueller, S.E. Basler, R. Müller, G.H. van Lenthe, Time-lapsed imaging of implant fixation failure in human

femoral heads, Med. Eng. & Phys. 35 (5) (2013), pp. 636–43. https://doi.org/10.1016/j.medengphy.2012.07.009

[3] C.K. Chao, C.C. Hsiao, Parametric study on bone screw designs for holding power, J. Mech. 22 (1) (2006), pp. 13–8. https://doi.org/10.1017/S1727719100000733

[4] A.E. Johnson, T.S. Keller, Mechanical properties of open-cell foam synthetic thoracic vertebrae, J. Mater. Sci. Mater. Med. 19 (3) (2008), pp. 1317–23. doi:10.1007/s10856-007-3158-7

[5] G. Menges, F. Knipschild, Estimation of mechanical properties for rigid polyurethane foams, Polym. Eng. Sci. 15 (8) (1975), pp. 623-27. doi:10.1002/pen.760150810

[6] L.J. Gibson, M.F. Ashby, G.S. Schajer, C.I. Robertson, The Mechanics of Two-Dimensional Cellular Materials, Proc. R. Soc. A. Math. Phys. Eng. Sci. 382 (1782) (1982), pp. 25–42. doi:10.1098/rspa.1982.0087

[7] L.J. Gibson, M.F. Ashby, The Mechanics of Three-Dimensional Cellular Materials, Proc. R. Soc. A. Math. Phys. Eng. Sci. 382 (1782) (1982), pp. 43–59. doi:10.1098/rspa.1982.0088

[8] J. Szivek, J. Thompson, J. Benjamin, Characterization of three formulations of a synthetic foam as models for a range of human cancellous bone types, J. Appl. Biomater. 6 (2) (1995), pp. 125–8. doi:10.1002/jab.770060207

[9] P.S.D. Patel, D.E.T. Sheperd, D.W.L. Hukins, Compressive properties of commercially available polyurethane foams as mechanical models for

osteoporotic human cancellous bone, BMC Musculoskeletal Disorders 9 (2008), pp. 137. doi:10.1186/1471-2474-9-137

[10] S. Gómez, M.D. Vlad, J. López, M. Navarro, E. Fernández, Characterization and three-dimensional reconstruction of synthetic bone model foams, Mater. Sci. Eng. C 33 (6) (2013), pp. 3329–35. doi:10.1016/j.msec.2013.04.013

[11] Y. Zhao, K.A. Robson Brown, Z.M. Jin, R.K. Wilcox, Trabecular level analysis of bone cement augmentation: A comparative experimental and finite element study, Ann. Biomed. Eng. 40 (10) (2012), pp. 2168–76. doi:10.1007/s10439-012-0587-3

[12] S. Youssef, E. Maire, R. Gaertner, Finite element modelling of the actual structure of cellular materials determined by X-ray tomography, Acta Mater. 53 (3) (2005), pp. 719–30. doi:10.1016/j.actamat.2004.10.024

[13] M.S. Thompson, I.D. McCarthy, L. Lidgren, L. Ryd, Compressive and shear properties of commercially available polyurethane foams, J. Biomech. Eng.-T ASME 125 (5) (2003), pp. 732–34. doi:10.1115/1.1614820

[14] L. Marsavina, D.M. Constantinescu, E. Linul, T. Voiconi, D.A. Apostol, Shear and mode II fracture of PUR foams, Eng. Fail. Anal. 58 (2) (2015), pp. 465–76. doi:10.1016/j.engfailanal.2015.05.021

[15] L. Marsavina, D.M. Constantinescu, E. Linul, F.A. Stuparu, D.A. Apostol, Experimental and numerical crack paths

in PUR foams, Eng. Fract. Mech. 167 (2016), pp. 68–83. doi:10.1016/j.engfracmech.2016.03.043

[16] H. Jin, W.Y. Lu, S. Hong, K. Connelly, Fracture Behavior of Polyurethane Foams, Proc. 2007 SEM Annu. Conf. Expo. Springfield, Massachusetts, June 4-6, 2007. doi:10.1115/IMECE2007-42732

[17] F.P. Chiang, Y. Ding, Size effect on stress-strain relation of neat polyurethane foam, Compos. Part. B Eng. 39 (1) (2008), pp. 42-9. doi:10.1016/j.compositesb.2007.02.011

[18] M.A. Sutton, J.J. Orteu, H. Schreier, Image correlation for shape, motion and deformation measurements: basic concepts, theory and applications 2009, Springer Science + Business Media (233 Spring street, New York, NY 10013, USA). ISBN: 9780387787473. https://doi.org/10.1007/978-0-387-78747-3

[19] B.K. Bay, Texture correlation: a method for the measurement of detailed strain distributions within trabecular bone, J. Orthop. Res. 13 (1995), pp. 256–67. https://doi.org/10.1002/jor.1100130214

[20] R. Belda, M. Palomar, J.L. Peris-Serra, A. Vercher-Martínez, E. Giner, Compression failure characterization of cancellous bone combining experimental testing, digital image correlation and finite element modeling, Int. J. Mech. Sci. 165 (2020), pp. 105213. https://doi.org/10.1016/j.ijmecsci.2019.105213

[21] B. Koohbor, S. Ravindran, A. Kidane, Effects of cell-wall instability and local failure on the response of closed-cell polymeric foams

subjected to dynamic loading, Mech. Mater. 116 (2018), pp. 67–6. http://dx.doi.org/10.1016/j.mechmat.2017.03.017

[22] G. Pyka, G. Kerckhofs, J. Schrooten, M. Wevers, The effect of spatial micro-CT image resolution and surface complexity on the morphological 3D analysis of open porous structures, Mater. Charact. 87 (2014), pp. 104–15. doi:10.1016/j.matchar.2013.11.004

[23] Sawbones catalogue. https:// www.sawbones.com / products/ biomechanical /biomechanical-test-materials.html

[24] K. Ün, G. Bevill, T.M. Keaveny, The effects of side-artifacts on the elastic modulus of trabecular bone, J. Biomech. 39 (2006), pp. 1955-63. https://doi.org/10.1016/j.jbiomech.2006.05.012

[25] A. Odgaard, F. Linde, The underestimation of Young's modulus in compressive testing of cancellous bone specimens, J. Biomech. 24 (8) (1991), pp. 691–98. https://doi.org/10.1016/0021-9290(91)90333-I

[26] T.M. Keaveny, R.E. Borchers, L.J. Gibson, W. Hayes, Theoretical analysis of the experimental artifact in trabecular bone compressive modulus, J. Biomech. 26 (4-5) (1993), pp. 599–607. https://doi.org/10.1016/0021-9290(93)90021-6

[27] R. Hambli, Micro-CT finite element model and experimental validation of trabecular bone damage and fracture, Bone 56 (2013), pp. 363–74. https://doi.org/10.1016/j.bone.2013.06.028

[28] J. Lemaitre, A continuous damage mechanics model for ductile fracture, J. Eng. Mater. Technol. 107 (1985), pp. 83–9. https://doi.org/10.1115/1.3225775

[29] D.L. Kopperdahl, T.M. Keaveny, Yield strain behavior of trabecular bone, J. Biomech. 31 (1998), pp. 601–8. https://doi.org/10.1016/S0021-9290(98)00057-8

[30] G.L. Niebur, M.J. Feldstein, J.C. Yuen, T.J. Chen, T.M. Keaveny, High-resolution finite element models with tissue strength asymmetry accurately predict failure of trabecular bone, J. Biomech. 33 (2000), pp. 1575–83. https://doi.org/10.1016/S0021-9290(00)00149-4

[31] H.H. Bayraktar, E.F. Morgan, G.L. Niebur, G.E. Morris, E.K. Wong, T.M. Keaveny, Comparison of the elastic and yield properties of human trabecular and cortical bone tissue, J. Biomech. 37 (2004), pp. 27–35. doi:10.1016/S0021-9290(03)00257-4

[32] R. Carretta, E. Stüssi, R. Müller, S. Lorenzetti, Within subject heterogeneity in tissue-level post-yield mechanical and material properties in human trabecular bone, J. Mech. Behav. Biomed. 24 (2013); pp. 64–73. http://dx.doi.org/10.1016/j.jmbbm.2013.04.014

[33] D. Ulrich, B. van Rietbergen, A. Laib, P. Rüegsegger, The ability of three-dimensional structural indices to reflect mechanical aspects of trabecular bone, Bone 25 (1) (1999), pp. 55–60. https://doi.org/10.1016/S8756-3282(99)00098-8